Temperature-Measurements of the IGM in Virgo Cluster

TECHNISCHE UNIVERSITÄT DARMSTADT

Bachelor-Arbeit

Betreuer:
Prof. Diana Worrall (University of Bristol)

Institut für Kernphysik

vorgelegt von

Steffen Hauf

Dezember 2006

Contents

List of Figures

Chapter 1

Introduction

This project is about the intra cluster medium in the Virgo cluster of galaxies. Virgo is the cluster located closest to us. Determining a proper distance from Earth has not yet been achieved, its close proximity does not allow a distance measurement via redshift since some of the galaxies within it even have a relative velocity pointing toward us. Other measurements involving various methods such as the Tully-Fisher relation Fukugita M. Okamura (1993),Okamura (1997) or by magnitude Sandage (1998) derived distances ranging between 12 and 30 Mpc and being elongated along the line of sight. All these measurements still have a large uncertainty but the average distance can be approximated to be around 20 Mpc.

Being so close the Virgo Cluster covers a fairly large region of the visible sky with an angular extent of around 6 in radius. In the optical it is cataloged to contain 2096 galaxies distributed over an area of $\approx 140 deg^2$ and centered at $\alpha \approx 12^h 15^m$ and $\delta \approx 13$ Matsumoto (2000). It's gravitational center is near M87 which is by far the largest galaxy within the cluster.

This paper compares ICM temperatures obtained previously by X-ray spectral fitting to such obtained using the much higher resolution data from the Chandra satellite. The data used is based on previous observations which did not have the aim of examining the ICM gas. Thus only a small region around the galaxies on which the observations were centered on is analyzed. Throughout this paper the distance of Virgo is assumed to be 20Mpc with zero redshift.

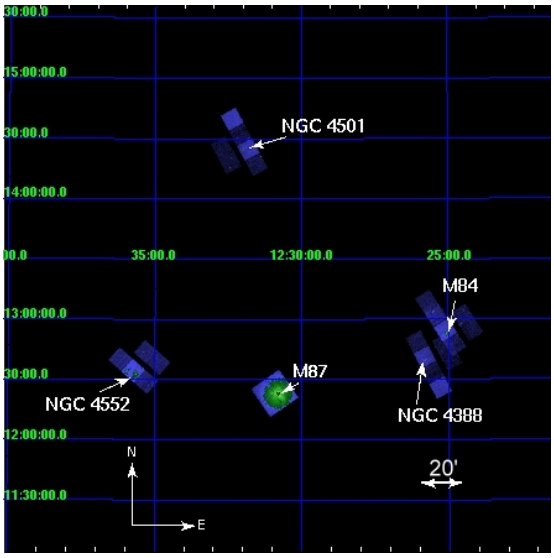

Figure 1.1: Mosaic showing the observations used along with M 87 as a point of reference.

Chapter 2

Virgo X-ray observations

2.1 History

The cluster had first been observed in the X-ray band by the Uhuru satellite and subsequently within the ROSAT all-sky survey. Based on observations from ASCA a map of the temperature distribution in a large area around M87 has been created in Matsumoto (2000). Over the last 40 years the spatial resolution of X-ray observatories has improved drastically. First satellites like Uhuru were sensitive only in one dimension, measuring the count rates of X-ray photons while the flew along their orbital path. They utilized proportional counters much like Geiger-Mueller counters for measurement. Uhuru which was the first satellite specifically designed for X-ray astronomy had a spatial resolution of 0.52. A great improvement was the 1978 Einstein satellite. Einstein first utilized a digital X-ray camera with a spatial resolution of 2" but with no spectral resolution. For spectral measurement the IPC instrument which again was a proportional counter had a resolution of 1'.

Rosat had a spatial spectral resolution of 25" and was the key instrument for the X-ray all sky survey. Finally the latest X-ray observatories Chandra and XMM Newton have spatial spectral resolutions below 2". A comparision of these different resolutions is shown in Figure A.1 in the appendix.

In 1972 observations with the Uhuru satellite led to the discovery of an extended X-ray source within Virgo Kellog (1972). This was confirmed by later observations and the center of the source was found to be near the central bright galaxy M87. Due to the low spatial and spectral resolution at that time the 1970s were dominated by the discussion whether the source was of thermal or non thermal origin. In 1978 A. Lawrence Lawrence (1978) still quotes a number of papers which seem to confirm that the spectrum from Virgo better fits a powerlaw (e.g. point source) than a thermal bremsstrahlung spectrum (e.g. extended source) because of M87 being a very dominant source in Virgo. With increasing resolution it was confirmed to be a thermal source and the center of emission was corrected to be offset from M87. In 1981 Lea et al. Lea (1981) found the X-ray emission to fit a thermal spectrum at 2.05 keV. With

further improved resolutions it was found that the ICM in Virgo is not isothermal, notably the region between M87 and M49 centered at R.A.=12h37m36s and decl. 918' has a much higher temperature of $\approx$ 4keV compared to the surrounding medium at 2 keV Kikuchi (2000). The highest resolution X-ray observatories to date, Chandra and XMM Newton now allow detection of temperature changes on much smaller scales further showing the non uniformity of the ICM.

2.2 Chandra observations

For this project a number of previous Chandra observations were used. All of them were centered on a galaxy within the cluster which usually completely covers one of the CCDs. The fact that these observations were not originally done for observing the ICM gas implies that only a small fraction of the total sky area covered by Virgo is included in the later analysis.

Further criteria for selecting observations were an exposure time greater than 10ks and that the instrument used was either ACIS-S or ACIS-I.

Each of the observation consists of four to six CCDs which have been individually analyzed. A mosaic of all observations used along with M 87 as a point of reference can be seen in Figure 1.1.

Chapter 3

Theoretical Background

3.1 Thermal Bremsstrahlung

The ICM within the Virgo cluster is filled with ionized gas, mostly Hydrogen which is the most abundant element in the universe. The cluster galaxies apply a strong gravitational pull on the gas particles. Because the gas is not being pulled in by the gravitational fields of the cluster galaxies, it is assumed to be in hydrostatic equilibrium:

$$\frac{dP}{dr} = -\rho(r)\frac{d\Phi}{dr} \tag{3.1}$$

$$P = \frac{\rho k T(r)}{\mu m_H} \tag{3.2}$$

where ρ is the gas density at radius r from the centre of gravity, k is the Boltzman constant, T the gas temperature, μ the mass partition and m_H the Hydrogen mass. The very strong gravitational pull from the cluster galaxies implies very high gas temperatures (Millions of Kelvin). The gravitational field within a Cluster have been found to comply with a King profile:

$$\Phi = \frac{9\sigma^2}{4\pi G r_c^2}(1 + r/r_c)^{-3/2} \tag{3.3}$$

Where σ is the central brightness and r_c is the core radius at $\sigma/2$. These equations are in principle sufficient for calculating the gas density profile of the cluster. This paper covers one of the preliminary steps for doing this calculation: determining the cluster gas temperature.

Even though this temperature can not be measured directly it can be derived from the radiation spectrum of the gas: ionized Hydrogen in the ICM is a very low density plasma at temperatures of millions of Kelvin. When electrons pass through the Coulomb field of these charged nuclei they emit Bremsstrahlung or as it is also often referred to: free-free radiation. This process of electron-proton Bremsstrahlung can

be approximated using classical physics and a dipole model. Quantum mechanics can be taken into account via the Gaunt factor, thus the Bremsstrahlungspectrum can be derived as shown in Wilms (N.d.):

Electron-electron or proton-proton interactions can not be described in this way though, because here the dipole moment is proportional to the center of mass, this is negligible for electron-proton radiation since the much heavier nucleus experiences almost no acceleration.

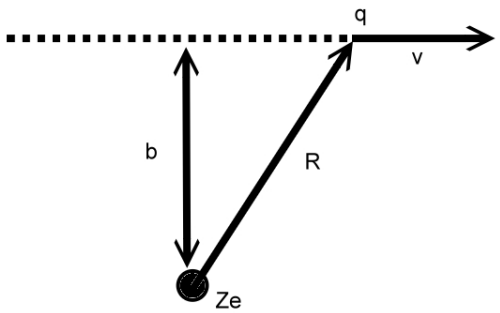

Figure 3.1: Straight line approximation of the electron path.

The electron path is approximated not to be influenced by the nucleus thus moves along a straight line with $z = vt$ as shown in Fig 3.1. And if the acceleration is mostly perpendicular to the motion:

$$\ddot{x} = \frac{Z_i e^2}{m_e(b^2 + v^2t^2)} \tag{3.4}$$

Therefor the electron experiences an electric field of

$$E(t) = \frac{Z_i e^3 sin\Theta}{m_e c^2 R(b^2 + v^2t^2)} \tag{3.5}$$

which gives in terms of frequency:

$$E(\omega) = (\frac{Z_i e^3 sin\Theta}{m_e c^2 R})(\frac{\pi}{bv})e^{-\omega b/v} \tag{3.6}$$

For the spectrum the Energy per unit area and frequency is necessary and integrated over a sphere with further approximation:

$$\frac{dW(b)}{d\omega} = \frac{8}{3\pi}(\frac{Z_i^2 e^6}{m_e^2 c^3}\frac{1}{(bv)^2} \tag{3.7}$$

for $b << v/\omega$ and 0 for $b >> v/\omega$.

One can further assume that the electron density n_e and the ion density n_i are constant within a region of suitable size.

Therefor the flux of electrons with velocity v incident on an ion is given by $n_e v$. The circular area element around any given ion is $2\pi bdb$. One can also assume that most collisions will be small angle and that the straight line approximation holds. Also boundry conditions are set so that quantum effects are small. A comparison with QED leads to g_{ff} which is the Gaunt factor:

$$g_{ff}(v,\omega) = \frac{\sqrt{3}}{\pi} ln(\frac{b_{max}}{b_{min}}) \tag{3.8}$$

One now relates the velocity of the electrons to the temperature of the gas by assuming that the velocity of the gas particles follows a Maxwell-Boltzmann distribution. This gives:

$$\frac{dW}{dVdtd\nu} = \frac{32\pi e^6}{3m_e c^3}(\frac{2\pi}{3m_e k})^{1/2} T^{-1/2} Z^2 n_e n_i e^{-h\nu/kT} \cdot \overline{g}_{ff} \tag{3.9}$$

with the velocity averaged Gaunt factor $\overline{g}_{ff}$.

Integrating over the entire frequency spectrum then gives the total power emitted per unit volume:

$$j^{ff} = \frac{dW}{dtdV} = (\frac{2\pi kT}{3m_e})^{1/2} \frac{32\pi e^6}{3hm_e c^3} Z^2 n_e n_i \overline{g}_B(T) \tag{3.10}$$

With $\overline{g}_B$ being the frequency average of g_{ff}.

Astronomical sources which emit Bremsstrahlung will at the same time also show Bremsstrahlung absorption. The effect of absorption can be calculated as shown in Wilms (N.d.) and results in a thermal Bremsstrahlung spectrum as shown in Figure 3.2. Note that the spectrum measured by a observatory will look quite different due to different instrument responses at varying energies which have to be corrected for.

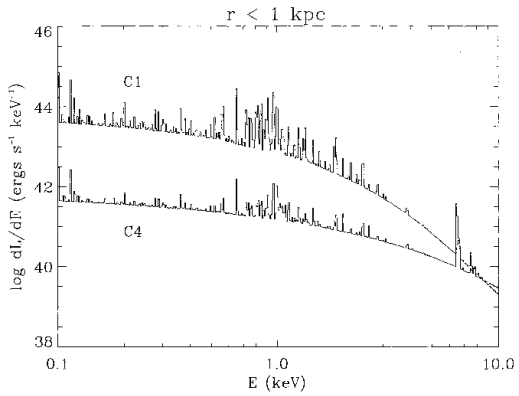

Figure 3.2: Theoretical X-Ray spectrum of cooling flow dominated bremsstrahlung and emission lines. Source: Wilms (N.d.)

3.2 Small Scale Cluster Clumping

Recent simulations have shown that clusters tend to clump on small scales due to shocks and acoustic disturbances. This causes density and therefor temperature variations. Because of this, models approximating a uniform ICM temperature and density for determining cluster mass scaling relations can show a significant amount of bias. Due to resolution issues these small scale clumps have not been observed in real clusters but are predicted by theoretical modes. This issue is important because with exact knowledge of temperature and mass of a cluster one can calculate the mass fraction of a cluster which has been found to be representative for the universe a whole. Knowledge of the mass fraction is an important prerequisite for solving the Friedman equation, whose solution determines the shape of the universe. It can be used as a lower limit for the baryon fraction and for constraining Ω_0 B. Mathiesen (1999).

Chapter 4

Data Preparation and Reduction

Although the Chandra website supplies preprocessed data for all observations We chose to use the raw data and then rerun the processing pipeline assuring that the same corrections and processing have been applied to all data used. When starting this project the current CIAO version in use was 3.2 so most pipeline processing was done with this version. If the newer version 3.3 was used this is explicitly mentioned. In addition tools from version 3.3 were used for later data reduction.

The raw data was processed as described in the ”Create a New Level 2 Event File” section of the ASIS analysis guides Chandra (N.d.). The procedures mentioned were written into a script for convenience but otherwise not altered.

Each observation was then divided into smaller regions. The region size was selected to include enough events for a later spectral analysis. Regions the size of one CCD chip proved to fulfill this requirement. Any regions covering more than one CCD would have caused problems with some of the CIAO tools used. The CCD containing the central bright source of an observation (note: the observations in use were earlier done for observing the galaxies not the gas) was divided into smaller regions because of the higher event rate. Mostly this CCD was divided into two or four regions. The region mapping scheme used is illustrated in Figure 4.1

Point sources which could be identified by eye were masked out before any further analysis was done. Leaving events related to point sources within the spectrum would have complicated the later fitting procedures. our tool of choice for doing this was DS9. In the further proceeding the term source will be used for the gas observed. Point sources will be referred to explicitly.

In a next step the source and background spectra were extracted for each of the previously created regions. Because the gas we are observing fills the entire observation area it was impossible to define separate background regions. Instead we decided to use the blank sky files as included in the CALDB. These files are strongly processed but still based on observation data so that they model the different backgrounds at different sky coordinates. See M. Markevitch’ ’cookbook for using ACIS background files’ Markevitch (2005) for details. We used the tool `acis_background_lookup` to find the files corresponding with a region within the CALDB. These background

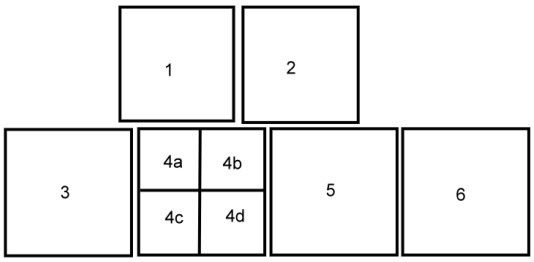

Figure 4.1: Scheme of region mapping. This numbering scheme was applied to all ACIS-S observations regardless of the orientation. Chip subdevisions were either 2 regions or 4 regions (as shown here).

files along with the source regions were then run through the `specextract` tool. This causes errors with some of the older background files due to improper set good time intervals (GTIs) within the background events file. By setting the GTI start to the exposure start of the source file and the GTI stop to GTI start + exposure time this problem was solved. It is to mention that doing this results in warnings in some of the tools that `specextract` runs but does not effect the resulting spectrum. Another preliminary step before using the background files was to assure that no bright flares were within the source data. This was done with the `lc_clean` script in Sherpa which defines the GTIs accordingly to mask out any flares. The bin times used while running `specextract` were set according to M. Markevitch' 'cookbook' Markevitch (2005)

4.1 Background Subtraction

We then tried different approaches for determining the the scaling factor of background compared with observation. The scaling value determined by `specextract` using a comparision of exposure time is much to low. Since the key spectral properties of the gas were likely to be found within an energy range of 0 to 5-6KeV we decided to try normalizing the background spectra in the upper energy band. The spectra of both source and background show very distinctive features in between 7 and 10 KeV.

In a first approach we tried fitting multiple Gaussian curves into the center region between the two peaks. This failed because the fits were very poor. A different approach was to scale by the distinctive peaks. Not wanting to use just one key feature of the spectra for the scaling factor we finally decided to scale by the mean value of both peaks leveling out smaller random discrepancies. To make this procedure reproducible we fitted a Gaussian to each of the peaks. The background fits were usually above 95 percent confidence level, but in case there were to few counts (as with most source fits) to get good statistics, but an inspection by eye showed that the fit was not running off we used them anyway. The exact procedure was to first fit to one of the peaks in the background spectrum then fit to the corresponding peak in the source spectrum with x_0

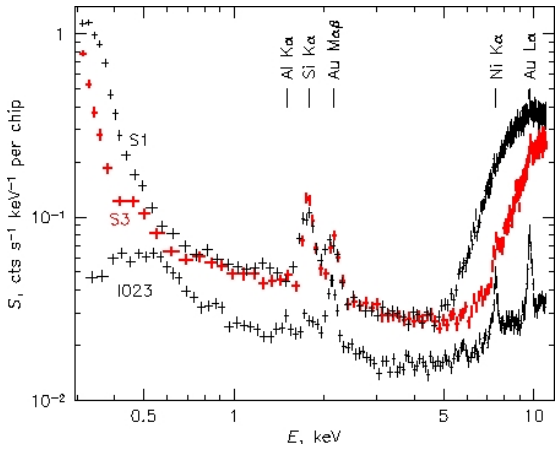

Figure 4.2: Energy spectra of the charged particle ACIS background with ACIS in the stowed position (a 50 ks exposure taken in September 2002; standard grade filtering, no VF filtering). Line features are due to fluorescence of material in the telescope and focal plane. Source: Chandra Proposer's Guide

fixed. The peak amplitudes were then divided to obtain a scaling factor. The formula used for this is:

$$s = \frac{A_{1,s}/A_{1,b} + A_{2,s}/A_{2,b}}{2} \tag{4.1}$$

where $A_{n,s}$ is the source amplitude and $A_{n,b}$ is the background amplitude.

This procedure is physically sensible since the higher energy regions of the spectrum are not dominated by "real" observation data but by instrument and particle background features. Since the instrument response to real X-ray events in these high regions is low the same quantitive features should appear in both background and source spectra. Therefor one can scale by these. It is to note that the peaks we used for scaling are due to fluorescence of the telescope material in the focal plane as seen in Figure 4.2.

The background scale was then set according to the obtained scaling factor for each region. It showed that neighboring regions usually had similar scaling factors and the scaling of the same chip across all observations was of same magnitude, which can be seen as a proof of concept in the sense that the scaling within one and all observations is consistent. The scaled background was subtracted from the source spectrum which was then regrouped, usually by count rates ranging from 75 to 150 counts, so that negative count rates due to the subtraction in the lower energy band from 1 to 5 keV were reduced. Sample calculations showed that this procedure of background subtraction implies statistic errors below 1.5%. We therefor ommit quoting these errors in later analysis due to their small effect in comparision to the errors caused by the actual spectral fit.

4.2 Spectral fitting

The boundary energies of 1 and 5 KeV were selected to exclude most of the particle and instrument background according to Figure 4.2. The remaining spectrum was then fitted to a combined absorption (`xstbabs`) and an `apec` thermal bremsstrahlung model (`xsapec`). The nH value for the absorption model was looked up with Colden and set accordingly. Further the Redshift within the thermo model was fixed to zero. Abundances and norm were allowed to run free. The original aim of fitting within a 95% confidence level could not be met by all fits. Some of the fits showed very poor statistics when grouping the spectrum by 50 counts or more. Fitting with different grouping values showed that the fitted gas temperature was the same within errors when using lower and higher grouping values. In such cases we grouped by lower values so that the 95% confidence level could be met. The fitting parameters and results can be found in Table A.1. Figures 4.3, 4.4 and 4.5 show fits of regions near NGC4388. These illustrate that it was not possible to exactly subtract the background from the source which becomes very clear at higher energies and lower count rates (emphasized also by the logarithmic scale). The scattering off the fit especially at these low count rates is very high. Figure 4.5 illustrates that with higher grouping values errors caused by the 'poor' background subtraction and instrument responses sum up. This along with lesser data points results in much poorer statistics. Figures 4.3 and 4.4 also show possible instrument related artifacts at arround 2keV which correspond to the peaks visible at these energies in Figure 4.2. Properly taking these into account might improve statistics but due to the limited time this could not be done. We only tried excluding these energies which did not result in better statistics due to less data points and minimally raised the fitted temperatures without exceeding the errors of fits including these energies.

Emphasizing again that a proper background subtraction with such low count rate proved very difficult we think our approach of accepting these 'noisy' spectra and fitting them despite this fact, with the aim of obtaining best possible statistics and not 'optical beauty' is reasonable. This is very debatable because just by looking at the fits one could to get the impression that the temperatures obtained could also be due to random noise. The fact that different grouping values result in almost the same temperatures and the fits following the overall properties of the observed spectrum seems to defy this criticism though. As shown in the following analysis the obtained temperature values also compare well to previous observations which again can be seen as a proof of concept.

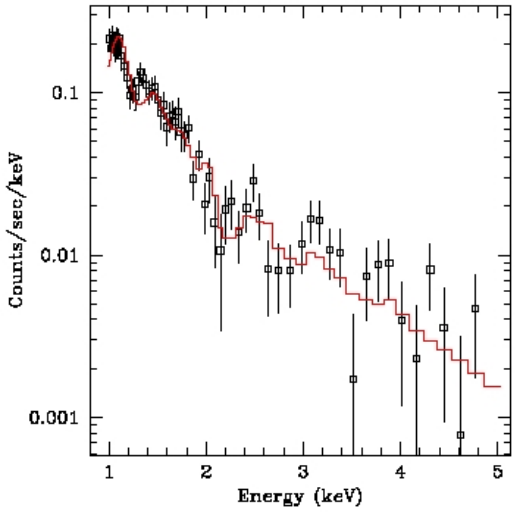

Figure 4.3: Spectral fit of chip 1 near galaxy NGC4388. Grouped by 50 counts.

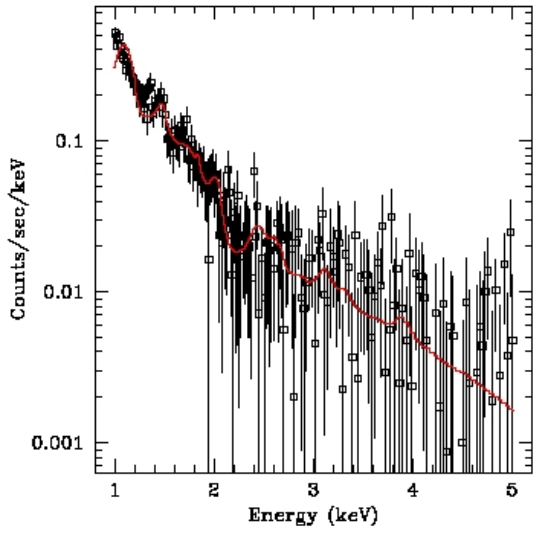

Figure 4.4: Spectral fit of chip 3 near galaxy NGC4388. Grouped by 10 counts.

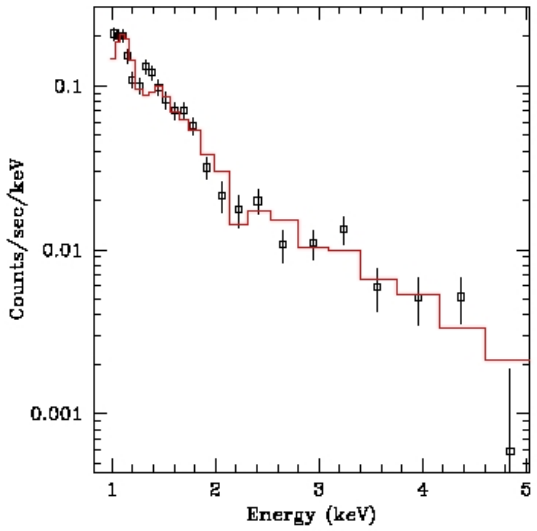

Figure 4.5: Spectral fit of chip 1 near galaxy NGC4388. Grouped by 150 counts.

Chapter 5

Results

5.1 ICM around NGC 4388

NGC 4388 is situated at R.A. $12^h25^m46.70^s$ and Decl. $+12^h39^m43.5^s$ which is to the east of M 87 an in close proximity of M 84. The observation we used for analysis is ObsID 1619 which was done with ACIS-S instrument and an exposure time of 20.23ks. The observation was divided into seven regions which can be seen in the temperature map of the observation. The region numbering scheme corresponds to the above mentioned. CCD chip 4 contained the galactic source so this chip was divided into two regions. Region 1 and 2 fitted well compared to the overall fitting problem. Region three showed very poor statistics which could only be resolved by choosing a grouping count of ten.

The observation shows a temperature increase toward the lower right corner. Especially the large increase between regions one and two was not expected and has to our knowledge not previously been observed on such small scales. A comparison with the results from Shibata et Al. Matsumoto (2000) show that there is no temperature change in global cluster scales present from which we assume that the ICM gas temperature may be variable on smaller scales which due to resolution issues could not be observed previously. The mean value of all fields combined in this observation is $2.50^{+0.44}_{-0.44}$keV. We calculated this assuming that all regions include approximately the same number of counts. The errors are calculated by standard error progression from the individual fields.

This value is slightly higher than the value of $2.35^{0.26}_{-0.26}$ keV obtained by Shibata et Al. Matsumoto (2000) in 2000 using ASCA observations and using a slightly larger field. The fact that both values match within the error boundaries gives confidence that previous temperature measurements are actually a superposition of much smaller scale temperature fluctuations and galaxy emission which was not masked out. When comparing the temperature gradients of our observations with those displayed in the temperature maps by Shabita one sees that they also match up. The temperature increases with decreasing declination in both cases.

5.2 ICM around NGC 4552

NGC 4552 is situated at R.A. $12^h35^m39.8^s$ and Decl. $+12^h33^m23^s$ which to the west of M 87. The observation used for analysis is ObsID 2072 take by ACIS-S at 55 ks exposure in VFAINT mode. The observation was divided into seven regions where chip four contained the bright galactic source and therefore was divided into two regions. In this observation it proved better to use higher grouping values due to very low count rates above 2keV. Regions one and two fit well with 250 counts per bin, region three was grouped by 350 counts. Region 4 did not fit within 95% confidence but given the previous results of very similar temperatures even with bad statistics we decided to include its temperature anyway. Regions five and six again fit well with grouping value of 150 and 50 counts per bin.

The observed temperatures do not vary much between neighboring regions except that region three is significantly cooler at $2.67^{+0.09}_{-0.09}$ keV than regions 4 at $4.40^{+0.66}_{-0.66}$ keV and 5 ($4.78^{+0.42}_{-0.42}$ kEV)located on the neighboring chips.

It seems as if the back illuminated chips detect a higher temperature than the surrounding but this is not consistent with the other observations we took.

The mean value of the observed temperature is $3.95^{+1.04}_{-1.04}$ compared to $2.28^{+0.12}_{-}0.08$keV obtained by Shabita by spectral fitting. The hardness ratio map by ShabitaMatsumoto (2000) shows slightly higher temperatures so the divergence of our values and the previously observed may be explicable to be caused by resolution issues of the older data. We find confidence in the fact that the basic temperature gradients again match well showing an increase to the south east and east.

5.3 ICM around NGC 4501

NGC 4501 is situated at R.A. $12^h31^m58.5^s$ and Decl. $+14^h25^m20^s$ which to the north of M 87. ObsId 2922 was used for analysis which was taken by ACIS-S with an exposure time of 18.1ks. The observation was divided into nine regions. Chips 1,2,3,5,6 each being covered by one region. Chip 4 being divided into 4 regions of which region a) could not be fitted properly.

We first tried fitting the observation with only one `xsapec` thermo model as done with the other observations. Even though the resulting statistics were reasonably good the fitted temperatures of $\geq$ 20keV were far too high for being only of thermal ICM origin.

This problem could be solved by adding a power law component (`powerlaw1d`) to the thermal model component. The powerlaw model was set to the default values with all parameters running freely. The absorption model was applied to both components. This approach produced reasonable temperatures around 1keV with good statistics. A comparison with the ASCA temperature maps shows that temperatures of $\approx$ 1keV have been previously measured inspiring confidence to the two component source model.

The obtained temperatures do not show any sharp cut offs or any dominant gradients within the observation.

The mean temperature of all regions is $1.22^{+2.05}_{-2.51}$keV with the large errors mainly due to the two component model used. The lower resolution value by ShabitaMatsumoto (2000) is $1.72^{+0.11}_{-0.12}$ with a one component model. Both datasets again show an increasing temperature to the south.

5.4 ICM around M 84

M 84 is situated at R.A. $12^h25^m03.6^s$ and Decl. $+12^h53^m14.1^s$ which to the east of M 87 and in close proximity of NGC 4388. The observation used is ObsID 803 observed with ACIS-S at 28.85ks exposure time. Single regions were mapped onto chips 1-4 and six whilst chip five was divided into two regions. Chip 4 did not fit the one component thermo model and was therefor excluded from analysis.

The observation is divided into two temperature zones. The regions east of M 84 have been fitted to temperatures of ≈4-4.5keV whereas regions lying to the west of M 84 are much cooler with temperatures between 2keV and 3keV. The Regions located on the same chip as M 84 show quite hard cut offs of temperature values. Between the larger regions on the other chips located further away from a galaxy the temperature gradient is not as steep.

Shabita observed temperatures of $2.35^{+0.26}_{-0.26}$keV and 0.78keV (fixed) with a two component thermo model where M 84 is located. The 0.78keV probably are due to IGM gas within M 84 producing a second underlying spectrum. We calculated a mean value of $3.56^{+1.12}_{-1.05}$keV. Within the errors both values are still comparable despite an apparent offset of 1.2keV. More important the temperature changes in the H.R. map match with those we detected. The temperature increase to the south east. Regions 5a and 5b lye exactly left to the temperature cut off in the H.R. map an have significantly lower temperatures than region 5c and 5d, which are on the other side of the cut.

Chapter 6

Discussion

Because of the much higher resolution the Chandra images have compared to the earliest temperature measurement described in the introduction there is not much sense in comparing our data with the 2.05keV mean temperature obtained in the late 1970s. The most detailed temperature maps to date are those calculate by Shabita et Al.Matsumoto (2000) in 2000. We will therefor compare our findings with theirs. In general it seems that we have obtained slightly higher temperature values in a given region than the earlier values. We suspect two main reasons for this. First, our method of background subtraction probably can still be tuned to be more accurate by combining multiple observations of similar coordinates thus increasing the count rates and source to background rates. We found that remaining background residuals in general increase the fitted temperature. Second we assume that due to the lower resolution some of the Shabita spectra may contain significant amounts of counts from IGM gas which could not be masked out to the same extent as the high resolution data allowed. Because of a smaller gravitational pull this gas is of lower temperature than the surrounding ICM and in result slightly decreases the earlier values. This is also suggested by MarkevitchMarkevitch (2002) when comparing XMM and Chandra data. The fact that the gradients of temperature changes in all our observations line up with those visible in the older temperature maps provides confidence that the 'absolute' value discrepancies may originate from one or both of the above described issues. For better comparison we overlaid the older temperature maps with our new results as shown in Figure A.3. Because we maintained the same coloring scheme as used by Shabita values below 1keV are not properly resolved in the image and are not displayed.

Chapter 7

Conclusion

We have shown that the high resolution X-ray images from the Chandra observatory allow a much smaller scaled analysis of the ICM structure than previously possible. Our observations provide evidence for previously not observed small scale temperature differences within the ICM which would have to be confirmed by the use of further observations. The background subtraction method we used for our analysis should be applicable within the entire cluster. To date we have only been able to analyze four fields due to a lack of time. These have so far resulted in data consistent in itself and with previous observations. In the further proceeding including more fields would give a more complete picture of the Virgo substructure. Especially the region between M87 and M49 which was observed to be the hottest region by Shabita would be an interesting target point. Due to the fact that all scripts and procedures for the analysis of additional field have now already been worked out their inclusion would be far less time consuming than the observations included so far. A more complete map of the Virgo substructure would also allow the verification of simulations predicting small scale clumping an could be useful for calculation of Ω_0.

references

B. Mathiesen, A.E. Evrard. 1999. *ApJ* 520:L21–L24.

Chandra. N.d. "ACIS Analysis Guide." http://asc.harvard.edu/ciao/guides/acis_data.html.

Fukugita M. Okamura, S. & Yasuda N. 1993. *ApJ* L13:412.

Kellog. 1972. *ApJ* 174:L65.

Kikuchi, K. 2000. "Detection of an X-ray hot region in the virgo cluster of galaxies with ASCA." *ApJ* 531:L95–L98.

Lawrence, A. 1978. "X-Ray emission from the Virgo Cluster and M87." *ApJ* 185:423–434.

Lea, S.M. 1981. "HEAO 1 High energy X-Ray observations of the Virgo cluster an A2142." *ApJ* 246:369–375.

Markevitch, M. 2002. "On the discrepancy between Chandra and XMM temperature profile for A1835." *www.arxiv.org/abs/astro-ph/0205333* .

Markevitch, M. 2005. "ACIS Background Cookbook." http://cxc.harvard.edu/cal/Acis/Cal_prods/bkgrnd/acisbg/COOKBOOK.

Matsumoto, R. Shibata K. Matsushita N. Y. Yamasaki T. Ohashi M. Ishida K. Kikuchi H. Böhringer H. 2000. "Temperature Map of the Virgo Cluster of Galaxies Observed with ASCA." *arXiv:astro-ph/0010380 v1* .

Okamura, Yasuda Fukugita &. 1997. *ApJS* 108:417.

Sandage, Federspiel Tammann &. 1998. *ApJ* 495:115.

Wilms, J. N.d. "Radiation Processes in Astronomy - Lecture Notes Chapt. 5.".

Appendix A

Appendix

A.1 Additional Figures

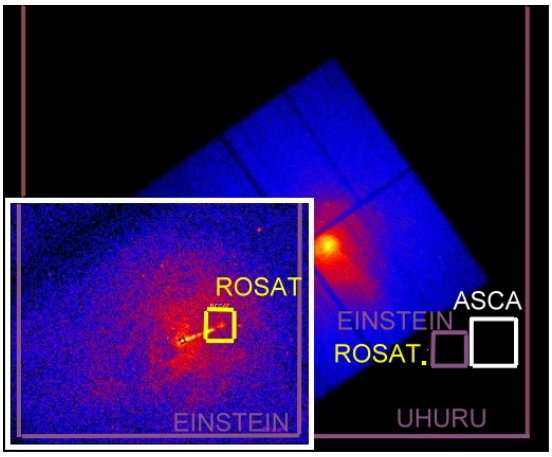

Figure A.1: The image shows M87 and the different spatial resolutions of some X-ray satellites. The inset image is a magnification of the center M87 along with Einstein and Rosat resolutions. One physical pixel in this image corresponds to the spatial resolution of Chandra (0.63”).

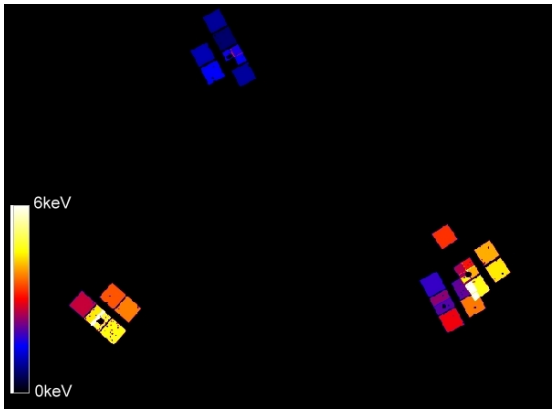

Figure A.2: Temperature map of all fields observed. Note that at overlapping regions the temperature is not displayed correctly. Orientation and position correspond to Fig 1.1

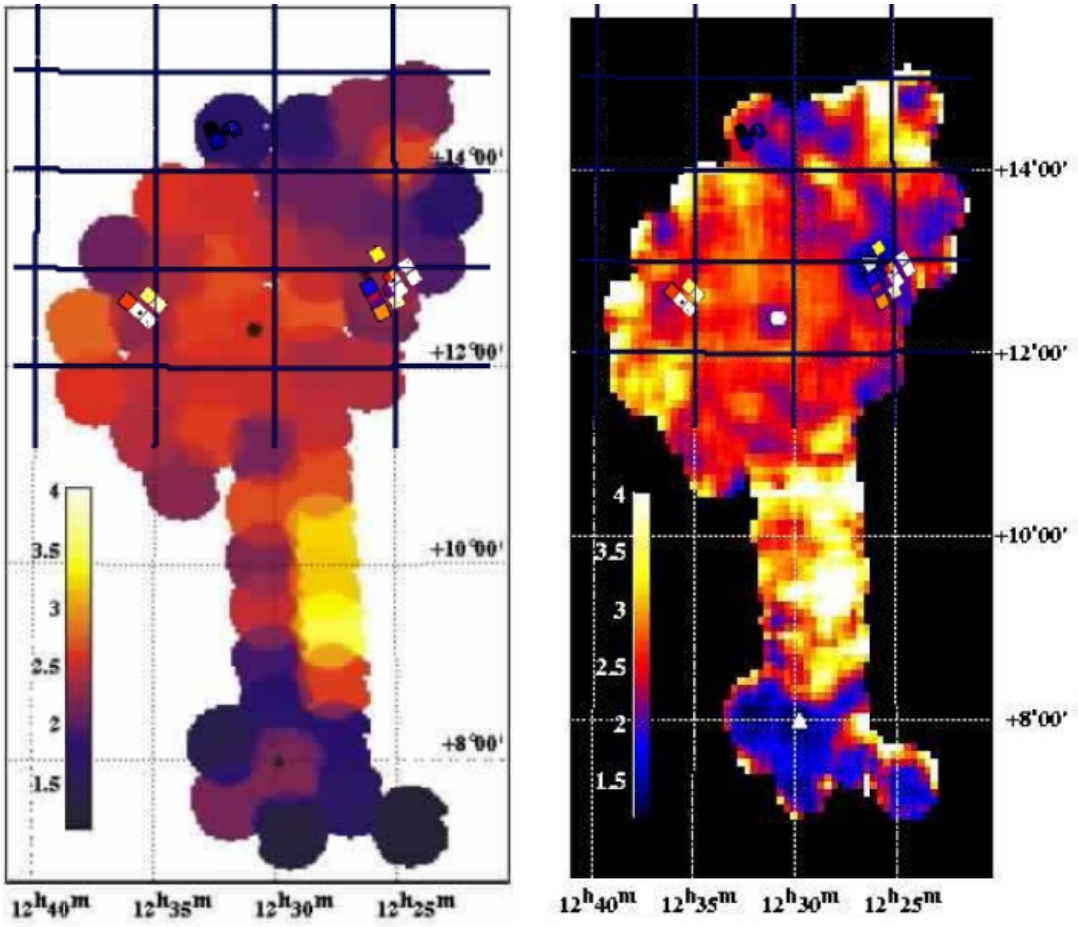

Figure A.3: (Left panel): Temperature map created by Shabita using spectral fitting overlaid with temperature map created from our results (smaller squares). The black circle marks the position of M87. (Right panel): Temperature map by Shabita calculated with hardness ratio. Again overlaid with a map displaying our data. The white circle marks the position of M87

A.2 Data log

Source	ObsID	PV	Region	T in keV†	nH††	scaling	N_g	χ^2(d.o.f)	remarks
NGC 4388	1619	3.2	chip1	$2.11^{+0.07}_{-0.07}$	2.71	0.247222	50	81.3(62)	
			chip2	$3.71^{+0.43}_{-0.43}$	2.71	0.211136	50	40.4(46)	
			chip3	$1.83^{+0.06}_{-0.06}$	2.71	0.683453	10	191.1(185)	[1]
			chip4a	$2.36^{+0.15}_{-0.15}$	2.71	0.36584	25	96.8(81)	
			chip4b	$2.04^{+0.08}_{-0.08}$	2.71	0.326335	25	135.5(111)	
			chip5	$2.93^{+0.22}_{-0.22}$	2.71	0.228523	20	101.5(105)	[1]
M 84	803	3.2	chip1	$4.03^{+0.38}_{-0.38}$	2.78	0.228971	50	66.2(65)	
			chip2	$4.39^{+0.66}_{-0.66}$	2.78	0.2253	50	36.7(56)	
			chip3	$3.30^{+0.50}_{-0.31}$	2.78	0.275585	25	128.3(115)	[2]
			chip5a	$3.11^{+0.25}_{-0.25}$	2.78	0.208841	50	56.1(45)	
			chip5b	$4.04^{+0.39}_{-0.39}$	2.78	0.168918	50	29.0(41)	
			chip5c	$2.55^{+0.12}_{-0.12}$	2.78	0.205726	50	56.6(53)	
			chip5d	$2.39^{+0.13}_{-0.13}$	2.78	0.171776	25	102.3(85)	
			chip6	$4.63^{+0.43}_{-0.43}$	2.78	0.230793	50	64.3(76)	
NGC 4552	2072	3.3	chip1	$3.50^{+0.52}_{-0.52}$	2.56	0.26822	250	29.5(25)	
			chip2	$3.76^{+0.26}_{-0.26}$	2.56	0.234691	250	29.4(26)	
			chip3	$2.67^{+0.09}_{-0.09}$	2.56	0.642729	350	61.9(19)	[3]
			chip4a	$4.40^{+0.66}_{-0.66}$	2.56	0.440241	350	31.0(19)	[3]
			chip4b	$4.78^{+0.42}_{-0.42}$	2.56	0.31476	50	100.7(101)	
			chip5	$4.60^{+0.35}_{-0.35}$	2.56	0.2534	50	54.2(50)	
NGC 4501	2922	3.2	chip1	$1.48^{+1.85}_{-1.85}$	2.48	0.39277	100	29.1(20)	[4]
			chip2	$1.05^{+0.37}_{-0.97}$	2.48	0.37683	100	16.5(17)	[4]
			chip3	$0.94^{+0.21}_{-0.21}$	2.48	0.766189	100	13.4(23)	[4]
			chip4b	$1.60^{+0.31}_{-0.31}$	2.48	0.182653	50	40.6(28)	[4]
			chip4c	$1.53^{+0.39}_{-0.99}$	2.48	0.28498	50	39.9(42)	[4]
			chip4d	$1.65^{+0.44}_{-0.31}$	2.48	0.25988	50	56.2(44)	[4]
			chip5	$0.64^{+0.21}_{-0.21}$	2.48	0.661033	50	30.1(45)	[4,5]
			chip6	$0.90^{+0.32}_{-0.83}$	2.48	0.596418	50	140.51(45)	[4]

Table A.1: PV: Pipeline version. N_g: Grouped by # of counts. †Statistical errors are quoted.††In units of $1 * 10^{20}/cm^2$.[1]Higher grouping values showed bad statistics but basically the same temperatures as with the low grouping value used. [2]Energies below 1.2 keV excluded. [3]Statistics did not match requirements (95% confidence) but due to consistency with other values fitted temperature was included. [4]Fitted to two component model: powerlaw for pointsource and bremsstrahlung for thermal. Power law was powlaw1d set to defaults all parameters allowed to run free. [5]While calculating scaling factor first background Gaussian did not fit. Peak was located by eye.

Danksagung

I would like to thank Prof. Diana Worrall for the excellent support and supervision during this project as well as the very helpful discussions and ideas which helped introduce me into this subject. I would like to thank my project partner Peter Otte without whom I would not have been able to get all the work done in time especially whilst calculating the spectra.

Furthermore I would like to thank Andreas Mooser and Daniel Pantel for their helpful discussions on statistics and Anja Zimmerer for proofreading this document.